Supporting information for

Hybrid Iron(II) Phthalocyaninoclathrochelates with Terminal Reactive Vinyl Group and their Organo-Inorganic Polymeric Derivatives: Synt hetic Approaches, X-ray Structures and Copolymerization with Styrene

Semyon V. Dudkin,[a] Alexander S. Chuprin,[a] Svetlana A. Belova,[a] Anna V. Vologzhanina,[a] Yan V. Zubavichus,[c] Polina M. Kaletina,[d] Inna K. Shundrina,[d] Elena G. Bagryanskaya,[d] and Yan Z. Voloshin[a,b,*]

[a]*Nesmeyanov Institute of Organoelement Compounds of the Russian Academy of Sciences, 28 Vavilova st., 119991 Moscow, Russia*

[b]*Kurnakov Institute of General and Inorganic Chemistry of the Russian Academy of Sciences, 31 Leninsky pr., 119991 Moscow, Russia*

[c]*Synchrotron Radiation Facility SKIF, Boreskov Institute of Catalysis of the Siberian Branch of the Russian Academy of Sciences, 1 Nikolskii pr., 6305590 Koltsovo, Russia*

[d]*Vorozhtsov Novosibirsk Institute of Organic Chemistry Siberian Branch of Russian Academy of Science, 9 Lavrentiev pr., 630090 Novosibirsk, Russia.*

Table S1. Isolated yields of the hybrid iron(II) phthalocyaninatoclathrochelates obtained using the *Methods A – C*

Complex	Transmetallation (*Method A*) Yield (%) last step/**total**	Cross-linking (*Method B*) Yield (%) last step/**total**	Template condensation (*Method C*) Yield (%)
$FeDm_3(B4\text{-}C_6H_4CH{=}CH_2)(ZrPc)$	55/**21**	b	**22**
$FeDm_3(B4\text{-}C_6H_4CH{=}CH_2)(HfPc)$	52[a]/**20**	b	**28**
$FeNx_3(B4\text{-}C_6H_4CH{=}CH_2)(ZrPc)$	b	45/**27**	**30**
$FeNx_3(B4\text{-}C_6H_4CH{=}CH_2)(HfPc)$	b	37/**22**	**48**

[a][S1]
[b]*We failed to obtain the corresponding complex precursor.*

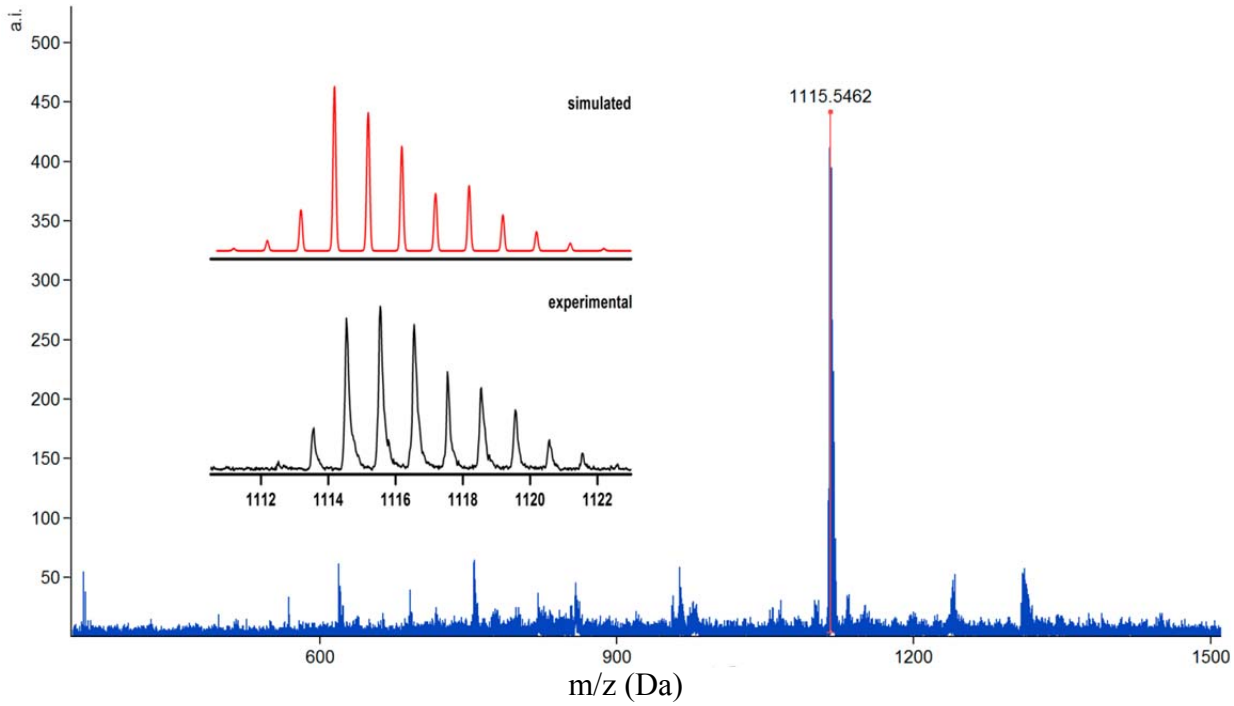

Figure S1. HR MALDI-TOF mass-spectrum of the hybrid complex **$FeDm_3$(B4-$C_6H_4CH=CH_2$)(ZrPc)**. Inset: the experimental and theoretically calculated isotopic distribution in its molecular ion.

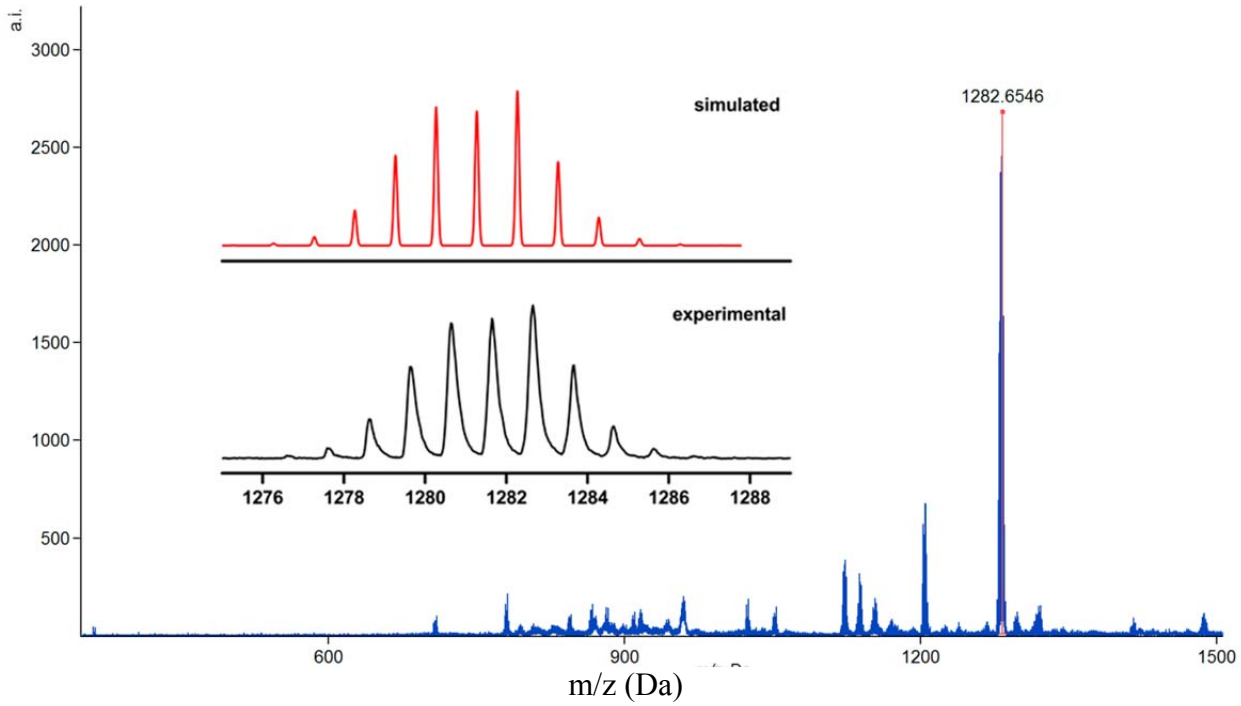

Figure S2. HR MALDI-TOF mass-spectrum of the hybrid complex **$FeNx_3$(B4-$C_6H_4CH=CH_2$)(HfPc)**. Inset: the experimental and theoretically calculated isotopic distribution in its molecular ion.

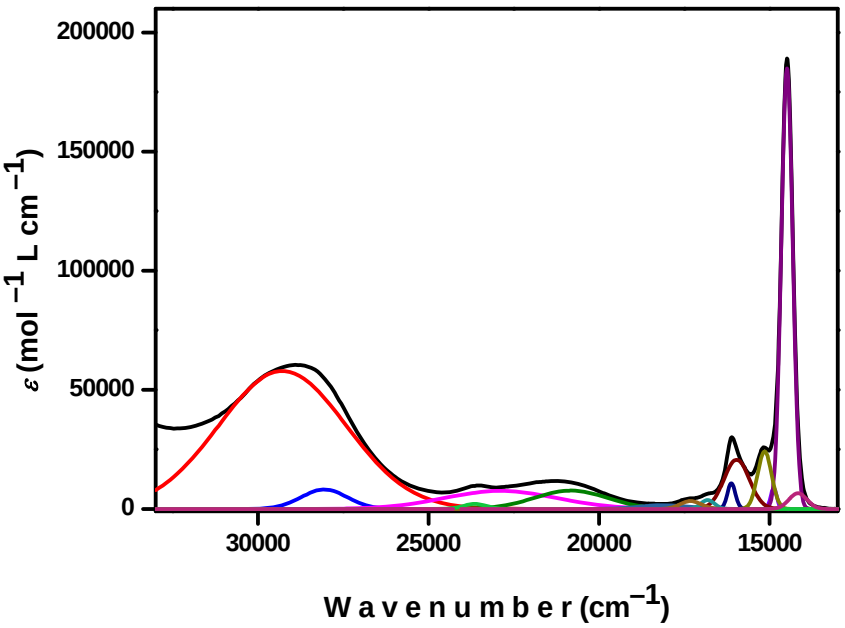

Figure S3. Solution UV-vis spectrum the complex **$FeDm_3$(B4-$C_6H_4CH=CH_2$)(ZrPc)** in 1,2-dichlorobenzene (shown in black line) and its deconvolution on the Gaussian components (shown in color lines).

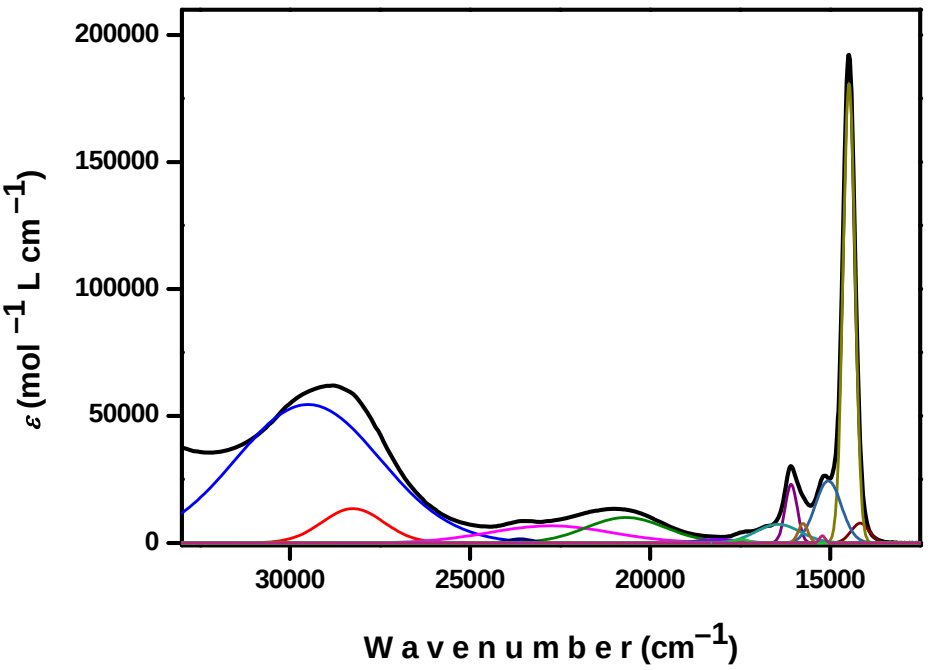

Figure S4. Solution UV-vis spectrum of the complex **$FeNx_3$(B4-$C_6H_4CH=CH_2$)(ZrPc)** in 1,2-dichlorobenzene (shown in black line) and its deconvolution on the Gaussian components (shown in color lines).

Crystal packings of the solvatomorphs of $FeDm_3$(B4-$C_6H_4CH=CH_2$)ZrPc)·

Using an algorithm from the Mercury 2020.1 program package, we compared the clusters of 20 molecules of the complex **$FeDm_3$(B4-$C_6H_4CH=CH_2$)ZrPc)**, which were extracted from the crystal structures of its solvatomorphs; the positions of the corresponding solvate molecules were not taken into account. This algorithm, that has been earlier described [S2, S3], confirmed that the crystals **$FeDm_3$(B4-$C_6H_4CH=CH_2$)ZrPc)**·0.5C_7H_{16}·1.5$CHCl_3$ and **$FeDm_3$(B4-$C_6H_4CH=CH_2$)HfPc)**·0.5C_7H_{16}·1.75$CHCl_3$ [S1] are isostructural; all their 20 phthalocyaninatoclathrochelate molecules can be overlaid with the average atomic deviations from each other of 0.068Å only. However, neither a pair of the crystals **$FeDm_3$(B4-$C_6H_4CH=CH_2$)(ZrPc)**·C_6H_6·C_8H_{18} and **$FeDm_3$(B4-$C_6H_4CH=CH_2$)(ZrPc)**·1.5$CHCl_3$, nor any of these solvatomorphs and the crystal **$FeDm_3$(B4-$C_6H_4CH=CH_2$)(ZrPc)**·0.5C_7H_{16}·1.5$CHCl_3$ form the similar packings. On the one hand, a similarity of the packings of clathrochelate fragments of the former pair of hybrid complexes is observed (Fig. S5, **b**). On the other hand, a substantial difference in the mutual shifts of their π-stacked neighboring molecules, forming a phthalocyaninatoclathrochelate dimer in the corresponding crystals, is clearly seen from this Figure. Contrary, in the case of a pair of the solvatomorps **$FeDm_3$(B4-$C_6H_4CH=CH_2$)(ZrPc)**· ·1.5$CHCl_3$ and **$FeDm_3$(B4-$C_6H_4CH=CH_2$)(ZrPc)**·0.5C_7H_{16}·1.5$CHCl_3$, a mutual orientation of their π-stacked phthalocyaninate macrocycles is similar, while the packings of their semiclathrochelate fragments in these crystals are different due to the different angles between their molecular Zr…Fe…B pseudoaxes (Fig. S5, **c**). Moreover, the use of the Solvate Analyzer tool from the Mercury 2020.1 program allowed us to calculate that in the case of the crystals of **$FeDm_3$(B4-$C_6H_4CH=CH_2$)(ZrPc)** containing benzene and *iso*-octane, chloroform, and heptane and chloroform solvate molecules, 16.4, 26 and 35.9% of crystal volumes of their unit cells are occupied by these molecules and their positions relative to the above phthalocyaninatoclathrochelate entities are also different. Indeed, in its two former crystals, they are located between the macrobicyclic frameworks of ditopic hybrid

molecules, while the solvate chloroform molecules in the crystal **$FeDm_3$(B4-$C_6H_4CH=CH_2$)(ZrPc)**·1.5$CHCl_3$ form a 3D-architecture (Fig. S5).

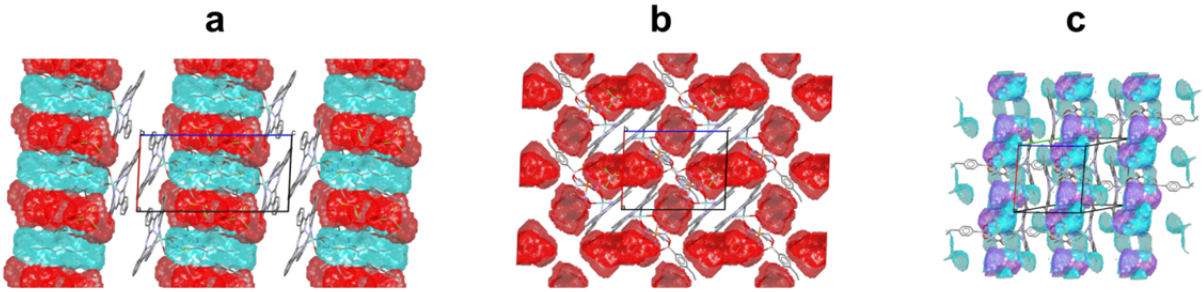

Fig. S5. Fragments of crystal packings of the solvatomorphs **FeDm$_3$(B4-C$_6$H$_4$CH=CH$_2$)(ZrPc)**·0.5C$_7$H$_{16}$·1.5CHCl$_3$ (**a**), **FeDm$_3$(B4-C$_6$H$_4$CH=CH$_2$)(ZrPc)**·1.5CHCl$_3$, (**b**) and **FeDm$_3$(B4-C$_6$H$_4$CH=CH$_2$)(ZrPc)**·C$_6$H$_6$·C$_8$H$_{18}$ (**c**). Volumes of their solvate chloroform, benzene and *n*-heptane molecules are depicted in red, violet and blue colors, respectively.

Table S2. Crystallographic data and experimental details for the vinyl-terminated iron(II) phthalocyaninatoclathrochelates

Parameter	**$FeDm_3(B4\text{-}C_6H_4CH{=}CH_2)ZrPc)\cdot$** $\cdot C_6H_6 \cdot C_8H_{18}$	**$FeDm_3(B4\text{-}C_6H_4CH{=}CH_2)ZrPc)\cdot$** $\cdot 1.5CHCl_3$	**$FeDm_3(B4\text{-}C_6H_4CH{=}CH_2)ZrPc)\cdot$** $\cdot 0.5C_7H_{16}\cdot 1.5CHCl_3$	**$FeNx_3(B4\text{-}C_6H_4CH{=}CH_2)ZrPc)\cdot$** $\cdot 2.125CHCl_3$
Empirical formula	$C_{66}H_{65}BFeN_{14}O_6Zr$	$C_{54.5}H_{43.5}BCl_6FeN_{14}O_6Zr$	$C_{57}H_{50.5}BCl_{4.5}FeN_{14}O_6Zr$	$C_{60.12}H_{49.12}BCl_{6.38}FeN_{14}O_6Zr$
Formula weight	1308.20	1361.11	1345.02	1447.63
Color, habit	Violet, prism	Red, plate	Violet, plate	Red, needle
Crystal size (mm)	0.16 × 0.12 × 0.11	0.26 × 0.23 × 0.08	0.36 × 0.34 × 0.09	0.37 × 0.06 × 0.05
a (Å)	12.904(3)	13.061(3)	12.0551(7)	12.875(3)
b (Å)	13.289(3)	13.926(3)	12.7677(7)	14.749(3)
c (Å)	17.715(4)	17.455(4)	22.1716(13)	19.981(4)
α (°)	92.23(3)	73.63(3)	74.184(3)	101.30(3)
β (°)	97.04(3)	87.99(3)	85.283(3)	104.72(3)
γ (°)	94.21(3)	76.02(3)	62.992(2)	96.60(3)
V (Å^3)	3003.4(11)	2953.9(12)	2921.9(3)	3543.8(14)
Crystal system	Triclinic	Triclinic	Triclinic	Triclinic
Space group	*P Ī, 2*	*P Ī, 2*	*P Ī, 2*	*P Ī, 2*
D_{cal}(g cm^{-3})	1.447	1.530	1.529	1.357
μ (mm^{-1})	0.669	0.943	5.875	0.909
Reflections collected	54921	64452	55496	58183
Independent reflections (R_{int})	12626 (0.106)	12733 (0.073)	11186 (0.169)	15466 (0.046)
Obs.refl./restraints/ parameters	10651/ 0 / 813	11881 / 0 / 755	9543 / 33 / 789	13642 / 48 / 894
R,[a] % [$F^2 > 2\sigma(F^2)$]	0.064	0.080	0.116	0.093
R_w,[b] % (F^2)	0.171	0.179	0.257	0.211
GOF	0.89	1.05	1.08	1.01
F(000)	1356	1379	1372	1470

[a] $R = \Sigma \big| |F_o| - |F_c| \big| / \Sigma |F_o|$. [b] $R_w = [\Sigma(w(F_o^2 - F_c^2)^2)/\Sigma(w(F_o^2))]^{1/2}$. [c] $\mathrm{GOF} = [\Sigma w(F_o^2 - F_c^2)^2/(N_{obs} - N_{param})]^{1/2}$

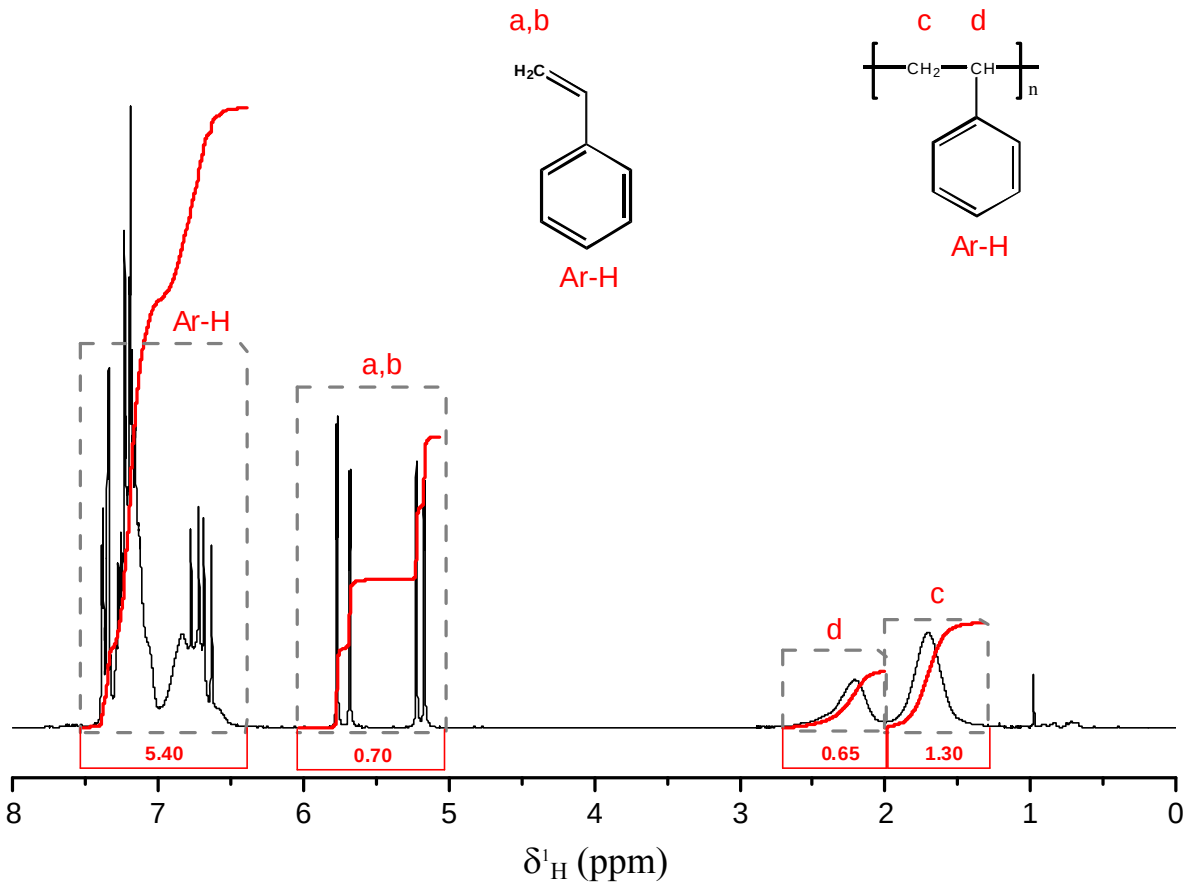

Fig. S6. C_6D_6 solution ^1H NMR spectrum of the polystyrene sample obtained by radical polymerization of styrene at 70°C for 28h (the degree of its conversion is equal to 65%).

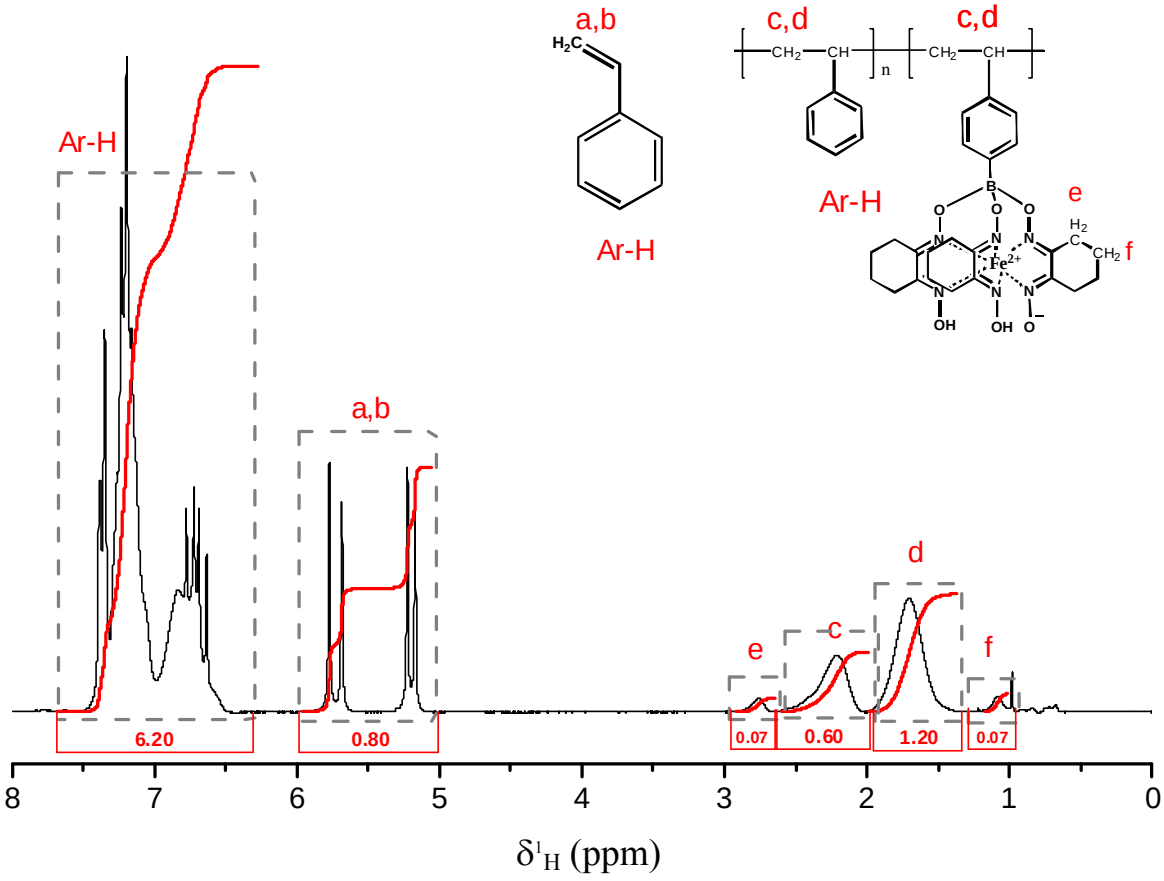

Fig. S7. C_6D_6 solution ^1H NMR spectrum of the copolymer sample obtained by radical polymerization of the styrene – $FeNx(HNx)_2(B4\text{-}C_6H_4CH{=}CH_2)$ system at 70°C for 28h (the degree of its conversion is equal to 60%).

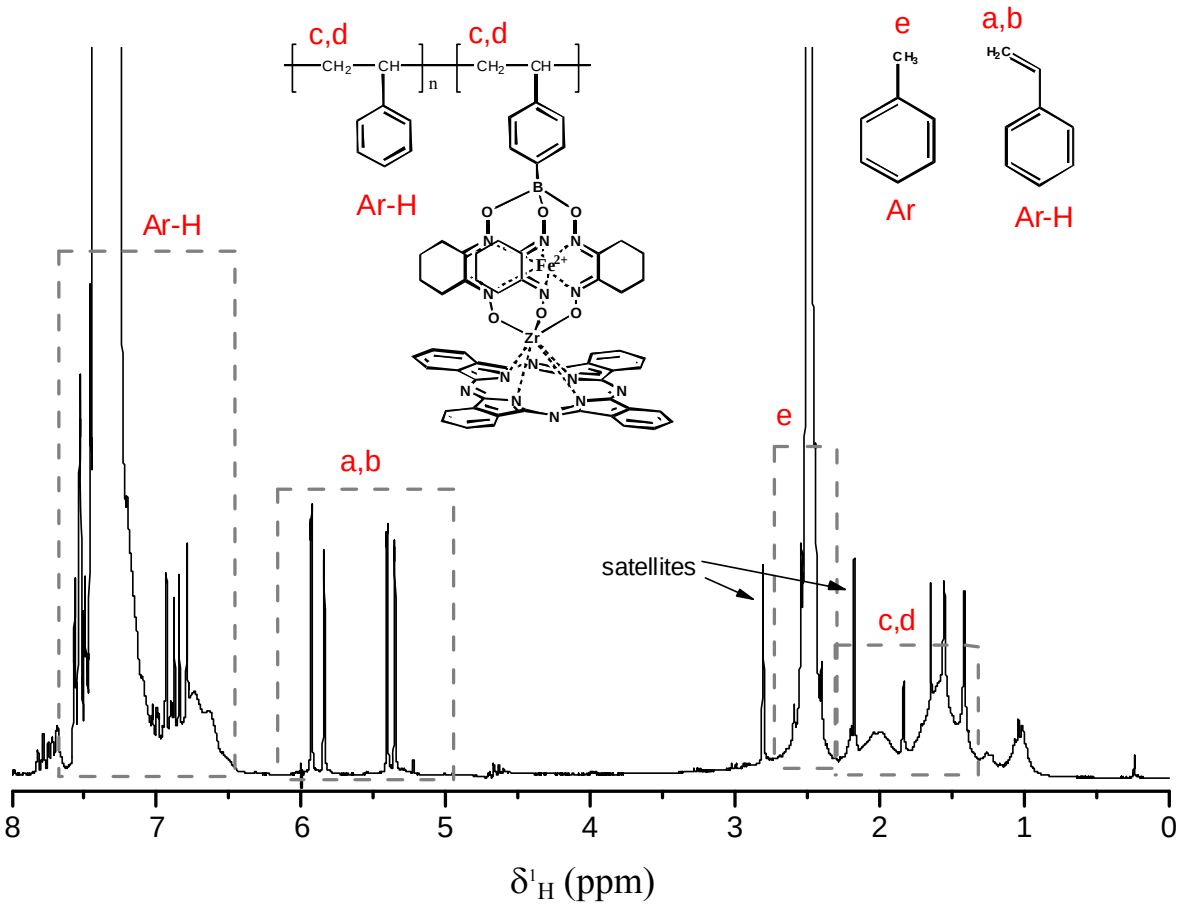

Fig. S8. C_7H_8 solution ^1H NMR spectrum of the polystyrene sample obtained by radical polymerization of the styrene – $FeNx_3(B4\text{-}C_6H_4CH{=}CH_2)(ZrPc)$ system at 70°C for 99h (the degree of its conversion is equal to 67%).

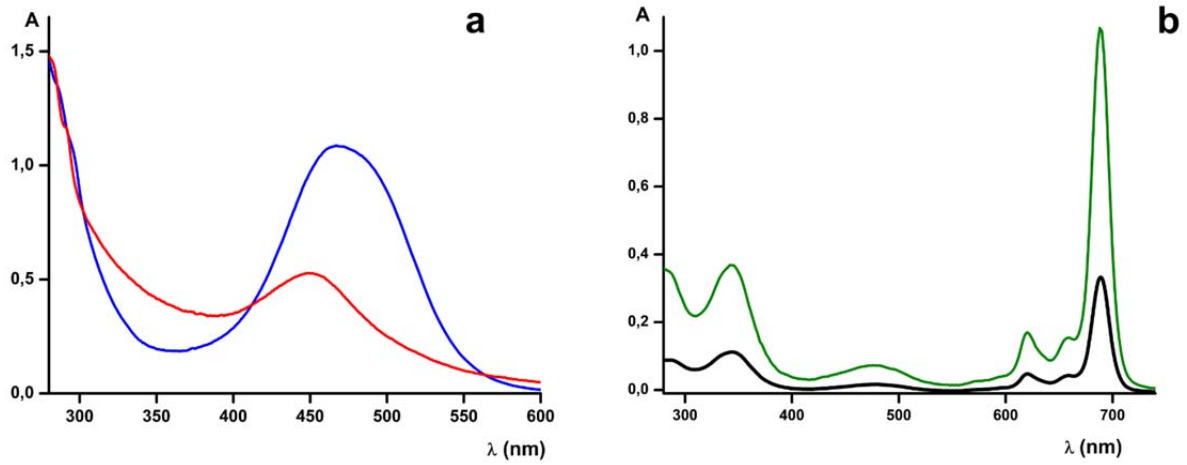

Fig. S9. (**a**) Solution UV-vis spectra of the copolymer **p(Sty–FeNx(HNx)$_2$(B4-C$_6$H$_4$CH=CH$_2$))** (shown in red line) and of its mononuclear metallocomplex precursor **FeNx(HNx)$_2$(B4-C$_6$H$_4$CH=CH$_2$)** (shown in blue line) in chloroform; (**b**) UV-vis spectra of the phthalocyaninatoclathrochelate-containing copolymer product **p(Sty – FeNx$_3$(B4-C$_6$H$_4$CH=CH$_2$)(ZrPc))** (shown in black line) and its phthalocyaninatoclathrochelate monomer precursor **FeNx$_3$(B4-C$_6$H$_4$CH=CH$_2$)(ZrPc)** (shown in green line).

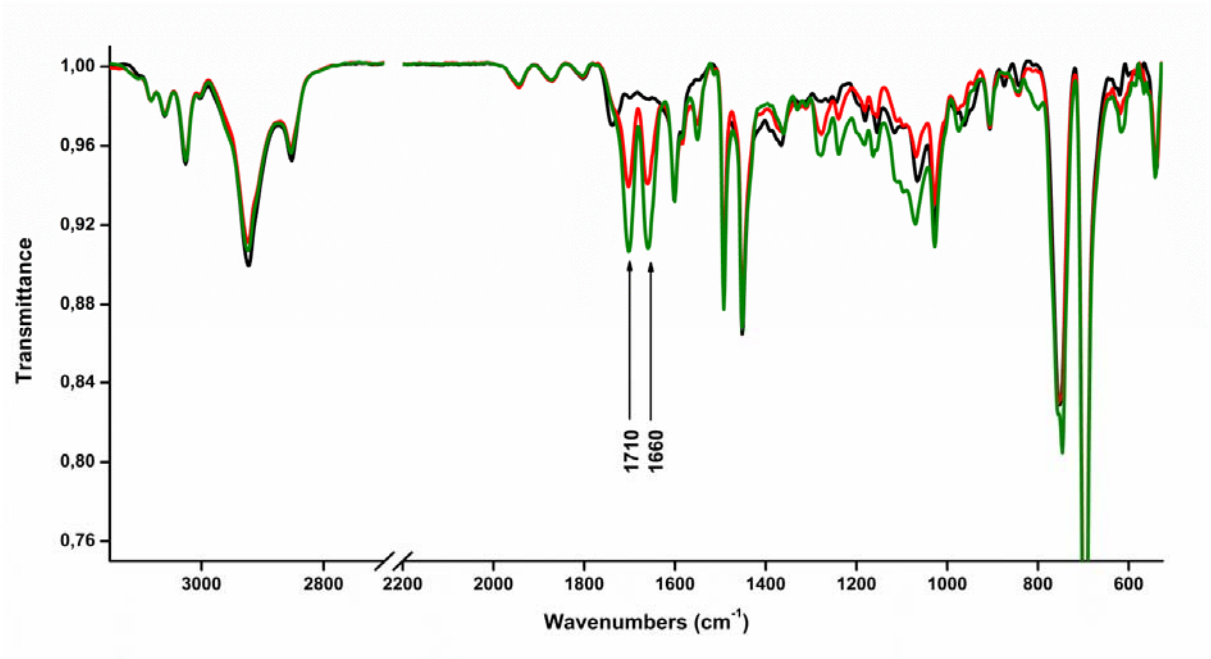

Fig. S10 FTIR spectra of the (co)polymer films of **pSty** (shown in black line), of **p(Sty–FeNx(HNx)$_2$(B4-C$_6$H$_4$CH=CH$_2$))** (shown in red line) and of **p(Sty–FeNx$_3$(B4-C$_6$H$_4$CH=CH$_2$) (ZrPc))** (shown in green line) after their UV-irradiation for 24 h.

Supporting Information References

S1. G. E. Zelinskii, S. V. Dudkin, A. S. Chuprin, A. A. Pavlov, A. V. Vologzhanina, E. G. Lebed, Y. V. Zubavichus and Y. Z. Voloshin, Synthesis, X-ray structure and reactivity of the vinyl-terminated iron(II) clathrochelate precursors and their cage derivatives with non-equivalent capping groups, *Inorg.Chim.Acta*, 2017, **463**, 29-35, DOI: 10.1016/j.ica.2017.04.011.

S2. S. L. Childs, P. A. Wood, N. Rodríguez-Hornedo, L. S. Reddy and K. I. Hardcastle, Analysis of 50 crystal structures containing carbamazepine using the materials module of mercury CSD, *Cryst Growth. Des*., 2009, **9**, 1869-1888, DOI: 10.1021/cg801056c.

S3. A. M. Reilly, R. I. Cooper, C. S. Adjiman, S. Bhattacharya, A. D. Boese, J. G. Brandenburg, P. J. Bygrave, R. Bylsma, J. E. Campbell, R. Car, D. H. Case, R. Chadha, J. C. Cole, K. Cosburn, H. M. Cuppen, F. Curtis, G. M. Day, R. A. DiStasio Jr, A. Dzyabchenko, B. P. van Eijck, D. M. Elking, J. A. van den Ende, J. C. Facelli, M. B. Ferraro, L. Fusti-Molnar, C.-A. Gatsiou, T. S. Gee, R. de Gelder, L. M. Ghiringhelli, H. Goto, S. Grimme, R. Guo, D. W. M. Hofmann, J. Hoja, R. K. Hylton, L. Iuzzolino, W. Jankiewicz, D. T. de Jong, J. Kendrick, N. J. J. de Klerk, H.-Y. Ko, L. N. Kuleshova, X. Li, S. Lohani, F. J. J. Leusen, A. M. Lund, J. Lv, Y. Ma, N. Marom, A. E. Masunov, P. McCabe, D. P. McMahon, H. Meekes, M. P. Metz, A. J. Misquitta, S. Mohamed, B. Monserrat, R. J. Needs, M. A. Neumann, J. Nyman, S. Obata, H. Oberhofer, A. R. Oganov, A. M. Orendt, G. I. Pagola, C. C. Pantelides, C. J. Pickard, R. Podeszwa, L. S. Price, S. L. Price, A. Pulido, M. G. Read, K. Reuter, E. Schneider, C. Schober, G. P. Shields, P. Singh, I. J. Sugden, K. Szalewicz, C. R. Taylor, A. Tkatchenko, M. E. Tuckerman, F. Vacarro, M. Vasileiadis, A. Vazquez-Mayagoitia, L. Vogt, Y. Wang, R. E. Watson, G. A. de Wijs, J. Yang, Q. Zhu and C. R. Groom, Report on the sixth blind test of organic crystal structure prediction methods, *Acta Crystallogr.B*, 2016, **72**, 439-459, DOI: 10.1107/S2052520616007447.